Manuscript version: Author's Accepted Manuscript
The version presented in WRAP is the author's accepted manuscript and may differ from the published version or Version of Record.

Persistent WRAP URL:
http://wrap.warwick.ac.uk/124043

How to cite:
Please refer to published version for the most recent bibliographic citation information. If a published version is known of, the repository item page linked to above, will contain details on accessing it.

Copyright and reuse:
The Warwick Research Archive Portal (WRAP) makes this work by researchers of the University of Warwick available open access under the following conditions.

© 2019 Elsevier. Licensed under the Creative Commons Attribution-NonCommercial-NoDerivatives 4.0 International http://creativecommons.org/licenses/by-nc-nd/4.0/.

Publisher's statement:
Please refer to the repository item page, publisher's statement section, for further information.

For more information, please contact the WRAP Team at: wrap@warwick.ac.uk.

An analytical solution to investigate the dynamic impact of a moving surface load on a shallowly-buried tunnel

Zonghao Yuan[a], Zhigang Cao[b,*], Yuanqiang Cai[a], Xueyu Geng[c], Xiaoqiang Wang[a]

[a]*College of Civil Engineering and Architecture, Zhejiang University of Technology, Hangzhou 310014, PR China*

[b]*College of Civil Engineering and Architecture, Zhejiang University, Hangzhou 310058, PR China*

[c]*School of Engineering, The University of Warwick, Coventry, CV4 7AL, UK*

Corresponding author*, Department of Civil Engineering and Architecture, Zhejiang University, Hangzhou 310027, PR China, E-mail addresses: caozhigang2011@zju.edu.cn, Telephone number: +86 571 88208774.

Abstract

In order to investigate the dynamic impact of a moving surface load on a shallow-buried tunnel, an analytical model of a tunnel embedded in an elastic half-space was proposed. The half-space and the tunnel structure were modeled as visco-elastic media and the moving surface load was simplified as a moving point load on the ground surface. Based on the fundamental solution for the isotropic elastic half-space system in Cartesian and cylindrical coordinates, the dynamic response of a shallowly-buried tunnel in a half-space generated by a moving surface load was obtained. The transformations between plane wave and cylindrical wave functions were used to facilitate the application of boundary conditions at the ground surface and the tunnel interface. It was found that the vibration of the shallowly-buried tunnel increases significantly as the load moving speed increases, and reaches a maximum value at a critical load velocity. The tunnel vibration can be greatly reduced as the buried depth increases, and can satisfy the requirement of vibration specification (ISO 04866-2010) after it exceeds the critical depth. The critical depth increases exponentially with the increase of the moving speed of the surface load.

Key words: surface moving loads; shallowly-buried tunnel; dynamic impact; analytical solution

1. Introduction

Underground tunnel is one of the most important transport infrastructures to reduce the traffic congestion pressure in densely populated cities. As most of them are constructed closely to buildings in urban areas, underground tunnels will inevitably cause nuisances to the environment nearby [1]. Meanwhile, the moving traffic on the ground surface may cause dynamic impact on the underground tunnel, including the excessive vibration of the lining and excessive dynamic stress on the tube, which threaten the stability of the tunnel structure during the excavation stage.

In the past decades, the ground vibrations caused by the operation of moving traffics have been extensively investigated [1-3], and it was found that significant nuisance could be caused to the environment by the operation of trains in the underground tunnel [2-3]. While the dynamic impact of moving traffics at ground surface on the underground tunnel remains unclear.

In fact, during the construction of underground tunnel in soft clay, the moving traffic on the ground surface may exert significant impact on the shallow-buried tunnel and even endanger the safety of tunnel. Soft clay is widely spread in eastern coastal areas of China, e.g., Shanghai, Hangzhou, Guangzhou and Hong Kong. The metro-lines were sometimes excavated very close to the existing highway roads or railway lines, the surface traffic loads may generate excessive dynamic stress on the primary lining before the soft soils have been fully supported by the secondary lining. As reported by Cai et al. [3], the operation of heavy truck on the highway surface was one of the major factors which caused the collapse of the Zizhi tunnel in Hangzhou when excavated in the mucky silty clay. In order to guarantee the safety of the tunnel excavation and the surface traffic operations, it is urgent to carry out research to evaluate the dynamic impact of surface traffic loads on the underground tunnel. Currently rare theoretical study has been conducted on the dynamic impact of moving surface loads on the underground tunnel.

In this paper, a three-dimensional analytical model of a circular tunnel buried in a visco-elastic half-space was established to investigate the impact of a surface moving load on the shallowly-buried tunnel. The velocity and stress response at the tunnel vault generated by a moving surface load are presented for different load speeds and load frequencies. Furthermore, the effects of lining thickness and tunnel depth on the tunnel's response due to the moving surface load were investigated.

2. Theoretical model and solutions

To investigate and evaluate the dynamic impact on the unground tunnel, an elastic dynamic model was established incorporating an elastic half-space and a circular tunnel as shown in Fig. 1. The ground was modelled as an isotropic viscoelastic material with a density ρ and Lamé constants λ and μ. The lining structure was modelled as a hollow cylinder with an inner radius a and an outer radius b. The lining has a density ρ_t and Lamé constants λ_t and μ_t. A moving surface load with a speed c and excitation frequency f_0 acts on the ground surface (x=d, y=0 m) and moves along the z direction.

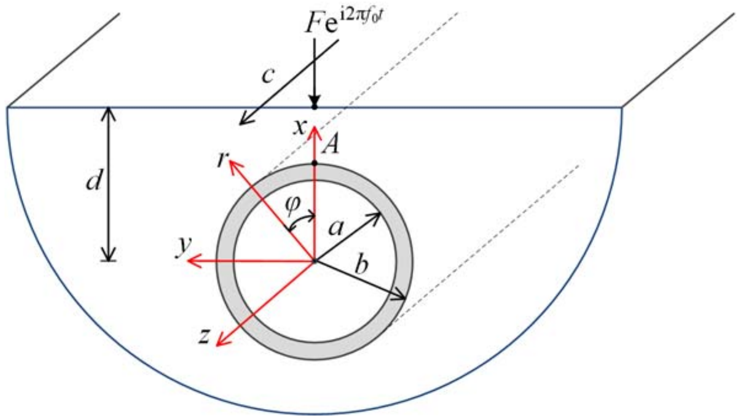

Fig. 1. The theoretical model of a tunnel buried in an elastic half-space

For the isotropic visco-elastic half-space, the governing equations are given as [4]:

$$(\lambda+2\mu)\nabla(\nabla\cdot\mathbf{u})-\mu\nabla\times(\nabla\times\mathbf{u})=\rho\ddot{\mathbf{u}} \tag{1}$$

where $\mathbf{u}$ is the displacement vector, ∇ is the Laplace operator and the dot over $\mathbf{u}$

denotes the differential with respect to the time t.

The traction on a plane with normal direction $\mathbf{e}_x$ is expressed as

$$\boldsymbol{t}^{(\mathbf{e}_x)}(\mathbf{u}) = \mathbf{e}_x \lambda \nabla \cdot \mathbf{u} + \mu \partial_x \mathbf{u} + \mu \nabla u_x \tag{2}$$

where $\mathbf{e}_x$, $\mathbf{e}_y$, $\mathbf{e}_z$ are unit vectors in Cartesian coordinate system.

The traction on a cylindrical surface with normal direction $\mathbf{e}_r$ is expressed as

$$\boldsymbol{t}^{(\mathbf{e}_r)}(\mathbf{u}) = \mathbf{e}_r \lambda \nabla \cdot \mathbf{u} + 2\mu \partial_r \mathbf{u} + \mu \mathbf{e}_r \times (\nabla \times \mathbf{u}) \tag{3}$$

where $\mathbf{e}_r$, $\mathbf{e}_\varphi$, $\mathbf{e}_z$ are the unit vectors in the cylindrical coordinate system.

The displacement field in a half space with a cavity is a sum of the displacement caused by down-going plane waves and that caused by outgoing cylindrical waves. The total displacement field can be written as

$$\mathbf{u} = \mathbf{u}_1 + \mathbf{u}_2 \tag{4}$$

where $\mathbf{u}_1$ is the displacement vector for down-going waves and $\mathbf{u}_2$ is the displacement vector for outgoing waves.

The displacement vectors $\mathbf{u}_1$ and $\mathbf{u}_2$ can be decomposed into three scalar potentials

$$\mathbf{u}_1 = \nabla \varphi_1 + \nabla \times (\mathbf{e}_z \varphi_2) + \nabla \times \nabla \times (\mathbf{e}_z \varphi_3) \tag{5a}$$

$$\mathbf{u}_2 = \nabla \chi_1 + \nabla \times (\mathbf{e}_z \chi_2) + \nabla \times \nabla \times (\mathbf{e}_z \chi_3) \tag{5b}$$

where φ_j is the potential for the down-going waves and χ_j is potential for the outgoing waves. The subscript j denotes the longitudinal (P, j=1), vertical transverse (SV, j=2) and horizontal transverse (SH, j=3) waves.

The potentials for down-going plane waves can be assumed as follows (Yuan et al. 2018)

$$\hat{\varphi}_1^- = A_1 \mathrm{e}^{\mathrm{i}(qz - h_\mathrm{p} x)} \cos py \tag{6}$$

$$\hat{\varphi}_2^- = A_2 \mathrm{e}^{\mathrm{i}(qz - h_\mathrm{s} x)} \cos py \tag{7}$$

$$\hat{\varphi}_3^- = A_3 \mathrm{e}^{\mathrm{i}(qz - h_\mathrm{s} x)} \sin py \tag{8}$$

where the hat "^" on the potentials denotes that the potentials are solved in the frequency-wavenumber (ω-q-p) domain; A_j are the unknowns determined from the boundary conditions; $k_{\mathrm{s,p}} = \omega / c_{\mathrm{s,p}}$ are the wave numbers with the shear and compressional wave velocity defined as $c_{\mathrm{s}} = \sqrt{\mu / \rho}$ and $c_p = \sqrt{(2\lambda + \mu) / \rho}$, respectively; $h_{\mathrm{s,p}} = \sqrt{k_{\mathrm{s,p}}^2 - q^2 - p^2}$ are wavenumbers in the x direction; p and q are wavenumbers in the y and z direction, respectively. The potentials for up-going waves $\hat{\varphi}_j^+$ (j=1, 2, 3) can be obtained by replacing -$h_{\mathrm{s,p}}$ with $h_{\mathrm{s,p}}$ in the Eqs. (6)-(8).

The displacement caused by the down-going waves can be obtained by substituting Eqs. (6)-(8) into Eq. (5a)

$$\hat{\mathbf{u}}_1 = \nabla \hat{\varphi}_1^- + \nabla \times (\mathbf{e}_z \hat{\varphi}_2^-) + \nabla \times \nabla \times (\mathbf{e}_z \hat{\varphi}_3^-)$$

$$= \begin{bmatrix} \hat{u}_{x1}^{1-} & \hat{u}_{x2}^{1-} & \hat{u}_{x3}^{1-} \\ \hat{u}_{y1}^{1-} & \hat{u}_{y2}^{1-} & \hat{u}_{y3}^{1-} \\ \hat{u}_{z1}^{1-} & \hat{u}_{z2}^{1-} & \hat{u}_{z3}^{1-} \end{bmatrix} \begin{bmatrix} A_1 \\ A_2 \\ A_3 \end{bmatrix} = \hat{\mathbf{U}}_1^- \begin{bmatrix} A_1 \\ A_2 \\ A_3 \end{bmatrix} \tag{9}$$

where $\hat{u}_{ij}^{1-}$ (i=x, y, z) represents the displacement component for the down-going plane waves.

The stress vector due to down-going waves can be obtained by substituting Eq. (9) into Eq. (2)

$$\hat{\boldsymbol{\sigma}}_1 = \begin{bmatrix} \hat{\sigma}_{x1}^{1-} & \hat{\sigma}_{x2}^{1-} & \hat{\sigma}_{x3}^{1-} \\ \hat{\sigma}_{y1}^{1-} & \hat{\sigma}_{y2}^{1-} & \hat{\sigma}_{y3}^{1-} \\ \hat{\sigma}_{z1}^{1-} & \hat{\sigma}_{z2}^{1-} & \hat{\sigma}_{z3}^{1-} \end{bmatrix} \begin{bmatrix} A_1 \\ A_2 \\ A_3 \end{bmatrix} = \hat{\mathbf{T}}_1^- \begin{bmatrix} A_1 \\ A_2 \\ A_3 \end{bmatrix} \tag{10}$$

where $\hat{\sigma}_{ij}^{1-}$ (i=x, y, z) denotes the stress component for the down-going plane waves.

The potentials for outgoing cylindrical waves can be assumed as

$$\tilde{\chi}_1^+ = \sum_{m=0}^{\infty} \tilde{\chi}_{1m}^+ = \sum_{m=0}^{\infty} B_{1m} H_m^{(1)}(g_{\mathrm{p}} r) \cos m\varphi \mathrm{e}^{\mathrm{i}qz} \tag{11}$$

$$\tilde{\chi}_2^+ = \sum_{m=0}^{\infty} \tilde{\chi}_{2m}^+ = \sum_{m=0}^{\infty} B_{2m} H_m^{(1)}(g_{\mathrm{s}} r) \sin m\varphi \mathrm{e}^{\mathrm{i}qz} \tag{12}$$

$$\tilde{\chi}_3^+ = \sum_{m=0}^{\infty} \tilde{\chi}_{3m}^+ = \sum_{m=0}^{\infty} B_{1m} H_m^{(1)}(g_{\mathrm{s}} r)\cos m\varphi \mathrm{e}^{iqz} \tag{13}$$

where the hat "~" on the potentials denotes that the potentials are solved in the frequency-wavenumber (ω-q) domain; $H_m^{(1)}$ is the Hankel function of the first kind, m=0, 1,….; $g_{\mathrm{s,p}} = \sqrt{k_{\mathrm{s,p}}^2 - q^2}$ is wavenumber in the r direction. The regular cylindrical vector wave functions $\tilde{\chi}_{jm}^0$ (j=1, 2, 3) can be obtained by replacing the Hankel function $H_m^{(1)}$ with a Bessel function $J_m^{(1)}$ in Eqs. (11)-(13).

The displacement due to the out-going waves can be obtained by substituting Eqs. (11)-(13) into Eq. (5b)

$$\tilde{\mathbf{u}}_2 = \sum_{m=0}^{\infty} (\nabla \tilde{\chi}_{1m}^+ + \nabla \times (\mathbf{e}_z \tilde{\chi}_{2m}^+) + \nabla \times \nabla \times (\mathbf{e}_z \tilde{\chi}_{3m}^+)) = \sum_{m=0}^{\infty} \begin{bmatrix} \tilde{u}_{r1}^{2+} & \tilde{u}_{r2}^{2+} & \tilde{u}_{r3}^{2+} \\ \tilde{u}_{\varphi 1}^{2+} & \tilde{u}_{\varphi 2}^{2+} & \tilde{u}_{\varphi 3}^{2+} \\ \tilde{u}_{z1}^{2+} & \tilde{u}_{z2}^{2+} & \tilde{u}_{z3}^{2+} \end{bmatrix} \begin{bmatrix} B_{1m} \\ B_{2m} \\ B_{3m} \end{bmatrix} = \sum_{m=0}^{\infty} \tilde{\mathbf{U}}_2^+ \begin{bmatrix} B_{1m} \\ B_{2m} \\ B_{3m} \end{bmatrix} \tag{14}$$

where $\tilde{u}_{ij}^{2+}$ (i=r, φ, z) represents displacement component for the outgoing cylindrical waves.

The stress vector due to the outgoing waves can be obtained by substituting Eq. (14) into Eq. (3)

$$\tilde{\boldsymbol{\sigma}}_2 = \sum_{m=0}^{\infty} \begin{bmatrix} \tilde{\sigma}_{r1}^{2+} & \tilde{\sigma}_{r2}^{2+} & \tilde{\sigma}_{r3}^{2+} \\ \tilde{\sigma}_{\varphi 1}^{2+} & \tilde{\sigma}_{\varphi 2}^{2+} & \tilde{\sigma}_{\varphi 3}^{2+} \\ \tilde{\sigma}_{z1}^{2+} & \tilde{\sigma}_{z2}^{2+} & \tilde{\sigma}_{z3}^{2+} \end{bmatrix} \begin{bmatrix} B_{1m} \\ B_{2m} \\ B_{3m} \end{bmatrix} = \sum_{m=0}^{\infty} \tilde{\mathbf{T}}_2^+ \begin{bmatrix} B_{1m} \\ B_{2m} \\ B_{3m} \end{bmatrix} \tag{15}$$

where $\hat{\sigma}_{ij}^{2+}$ represents stress component for the out-going plane waves (see Yuan et al. [5]).

In order to apply the boundary condition on the ground surface, the transformation of the outgoing waves to the up-going plane waves is required. The unit point load acting on the ground surface (x=d, y=0), $\boldsymbol{F} = \delta(z - ct)\delta(y)\mathrm{e}^{-\mathrm{i}2\pi f_0 t}\mathbf{e}_x$ can be expanded into an integral with respect to the wavenumber q

$$\boldsymbol{F} = \mathbf{e}_x \frac{1}{2\pi c} \int_{-\infty}^{\infty} dq \mathrm{e}^{\mathrm{i}qz} \delta(q - \frac{\omega - 2\pi f_0}{c}) \cdot \frac{1}{\pi} \int_0^{\infty} \cos py dp \tag{16}$$

In order to apply the boundary condition at the tunnel-soil interface, the down-going plane waves should be transformed to regular cylindrical waves. Combined with the boundary conditions at the surface and tunnel-soil interface, total displacement in the half-space is described with the cylindrical coordinates:

$$\mathbf{u}(\mathbf{r})=\int_{-\infty}^{\infty}\sum_{m=0}^{\infty}\left(\sum_{m'=0}^{\infty}\begin{bmatrix}\omega_{r1m'} & \omega_{r2m'} & \omega_{r3m'}\\ \omega_{\varphi1m'} & \omega_{\varphi2m'} & \omega_{\varphi3m'}\\ \omega_{z1m'} & \omega_{z2m'} & \omega_{z3m'}\end{bmatrix}\begin{bmatrix}B_{1m'}\\ B_{2m'}\\ B_{3m'}\end{bmatrix}-\begin{bmatrix}\tilde{u}_{r1}^{2(0)} & \tilde{u}_{r2}^{2(0)} & \tilde{u}_{r3}^{2(0)}\\ \tilde{u}_{\varphi1}^{2(0)} & \tilde{u}_{\varphi2}^{2(0)} & \tilde{u}_{\varphi3}^{2(0)}\\ \tilde{u}_{z1}^{2(0)} & \tilde{u}_{z2}^{2(0)} & \tilde{u}_{z3}^{2(0)}\end{bmatrix}\begin{bmatrix}T_{1m}\\ T_{2m}\\ T_{3m}\end{bmatrix}+\begin{bmatrix}\tilde{u}_{r1}^{2+} & \tilde{u}_{r2}^{2+} & \tilde{u}_{r3}^{2+}\\ \tilde{u}_{\varphi1}^{2+} & \tilde{u}_{\varphi2}^{2+} & \tilde{u}_{\varphi3}^{2+}\\ \tilde{u}_{z1}^{2+} & \tilde{u}_{z2}^{2+} & \tilde{u}_{z3}^{2+}\end{bmatrix}\begin{bmatrix}B_{1m}\\ B_{2m}\\ B_{3m}\end{bmatrix}\right)dq \tag{17}$$

The total displacement field in the lining structure is

$$\tilde{\mathbf{u}}_t(\mathbf{r})=\int_{-\infty}^{\infty}\sum_{m=0}^{\infty}\left(\begin{bmatrix}\tilde{u}_{r1}^{t(0)} & \tilde{u}_{r2}^{t(0)} & \tilde{u}_{r3}^{t(0)}\\ \tilde{u}_{\varphi1}^{t(0)} & \tilde{u}_{\varphi2}^{t(0)} & \tilde{u}_{\varphi3}^{t(0)}\\ \tilde{u}_{z1}^{t(0)} & \tilde{u}_{z2}^{t(0)} & \tilde{u}_{z3}^{t(0)}\end{bmatrix}\begin{bmatrix}C_{1m}\\ C_{2m}\\ C_{3m}\end{bmatrix}+\begin{bmatrix}\tilde{u}_{r1}^{t+} & \tilde{u}_{r2}^{t+} & \tilde{u}_{r3}^{t+}\\ \tilde{u}_{\varphi1}^{t+} & \tilde{u}_{\varphi2}^{t+} & \tilde{u}_{\varphi3}^{t+}\\ \tilde{u}_{z1}^{t+} & \tilde{u}_{z2}^{t+} & \tilde{u}_{z3}^{t+}\end{bmatrix}\begin{bmatrix}D_{1m}\\ D_{2m}\\ D_{3m}\end{bmatrix}\right)dq \tag{18}$$

The detail for the wave transformation and the definition of coefficients can refer to Yuan et al. [5,8].

3 Numerical results

3.1 Verification of the proposed approach

In order to verify this model, the comparisons between the present work and Hung and Yang [6] were presented. Hung and Yang [6] studied the vibrations of an elastic half-space generated by a moving surface load with semi-analytical methods. By reducing the radius of the buried tunnel to a=0.1m, the normalized displacement response, $u_z^*=(4\pi G/P)u_z$ (P is the load amplitude and G is the soil shear modulus) for the two models are presented in Fig. 2. It can be seen that the two results agree well.

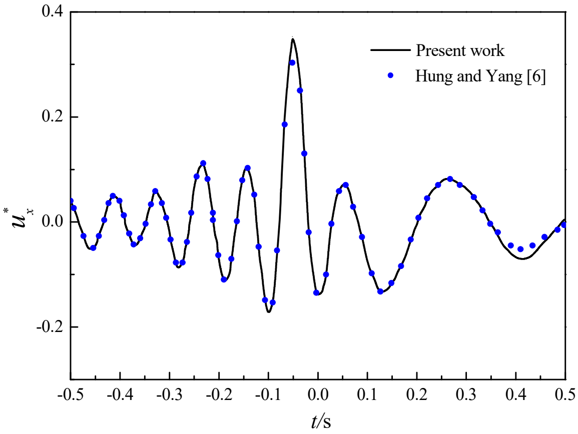

Fig. 2. Comparison with Hung and Yang [6]

3.2 Responses of a tunnel generated by a moving harmonic surface load

In this subsection the dynamic response of the tunnel generated by a unit moving harmonic load is investigated for different moving velocities. The amplitude of load is taken as 200kN which simulates heavy vehicles and the load frequency is taken as 5 Hz. The parameters for the elastic soil and the lining are listed in Tables 1 and 2, respectively. Unless otherwise specified, the tunnel has an outer radius of 5 m (b=5 m) with a thickness of 0.25 m (b-a), and a depth d=15 m.

Table 1 Parameters of half-space soil medium

Lamé constants of the ground, μ	1.2×10^7 N/m^2
Lamé constants of the ground, λ	3.7×10^7 N/m^2
Density of the half-space, ρ	1900 kg/m^3
Damping of the half-space, δ	0.05

Table 2 Parameters of lining structure

Lamé constants of lining, μ_t	1.9×10^{10} N/m^2
Lamé constants of lining, λ_t	2.88×10^{10} N/m^2
Density of lining, ρ_t	2400 kg/m^3
Damping of lining, δ	0.02

The point A (x=5 m, y=0 m, z=0 m) at the vault of the tunnel is chosen as the observation point, see in Fig. 1. The time history of the vertical displacement at point A caused by a moving harmonic load is plotted in Fig. 3, where t=0 s corresponds to the moment when the point load passes through the origin (z=0 m). Three load speeds c=20 m/s, 60 m/s and 100 m/s are used for the computations. As shown in Fig. 3(a), the vertical displacement at point A reach a peak value at t=0 s, and the corresponding maximum values are 2×10^{-4}m, 4×10^{-4}m and 7×10^{-4}m for the load speeds c=20m/s, 60m/s and 100m/s, respectively. It can be found that an increase in the load speed results in an obvious increase of the displacement response. Fig. 3(b) presents the corresponding frequency spectrum of the displacement response. When load speed is 20m/s, the frequency components distribute mainly in the range between 3Hz and 7Hz. As the load speed increases to 60m/s and 100m/s, the corresponding frequency components mainly distribute in the range of 1-10Hz and 0-15Hz. This is due to the well-known Doppler effects, and the frequency range can be calculated by $f_{cr}=f_0/2\pi(1\pm c/c_R)$ (f_{cr} is the upper and lower limit of the frequency range and c_R is the Rayleigh wave speed of the ground).

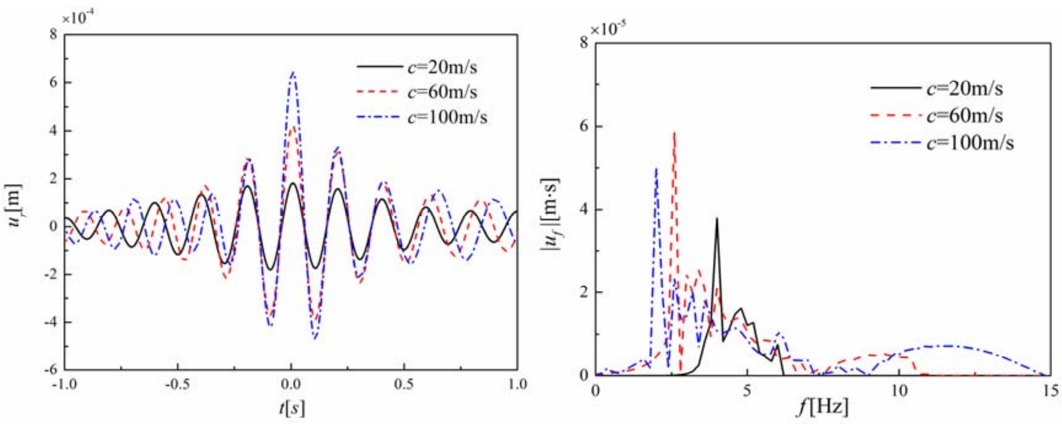

Fig. 3. The vertical displacement of the tunnel to a moving harmonic load: (a) time history, (b) frequency spectrum

Fig. 4 gives the vertical velocity response at the tunnel vault (point A) and radial stress responses around the tunnel periphery under different speed loads for a tunnel depth 15 m (d/b=3). As can be seen in Fig. 4(a), the maximum velocities are 5.3×10^{-3}m/s^2, 6.4×10^{-3}m/s^2 and 9×10^{-3}m/s^2 for c=20 m/s, 60 m/s and 100 m/s, respectively. The velocity of the lining increases apparently with the increase of loading speed. Another observation from Fig. 4(a) is that the peak-peak responses duration at the point *A* is shortened as the load speed increases. To investigate the spatial distribution of the stress response around the tunnel, the amplitude of the radial stress response at the soil-tunnel interface is displayed in Fig. 4(b). The load speed has a significant influence on the dynamic stress, especially at the vault of the tunnel.

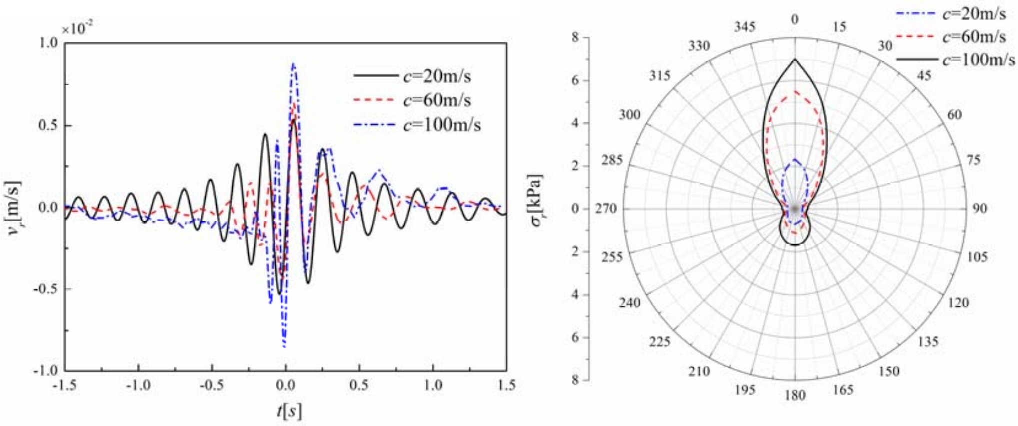

Fig. 4. Velocity and stress response of the tunnel to a moving harmonic load: (a) vertical velocity and (b) radial stress

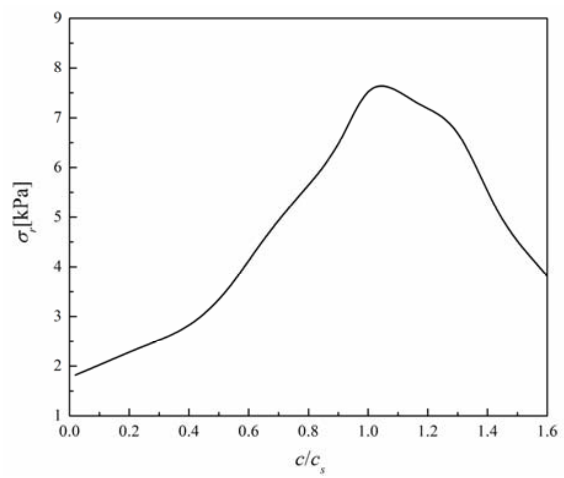

Fig. 5. The maximum radial stress at point *A* against the dimensionless load speed

Fig. 5 presents the maximum radial stress at the observation point *A* against the load speed to further investigate the load speed effect. The dimensionless load speed is selected as c/c_s, in which c_s is the shear wave speed of soil. As can be seen in Fig. 5, the maximum radial stress increases rapidly with load speed *c* and reach a sharp peak at a certain velocity, which is defined as the critical velocity of the tunnel-soil system. The critical velocity is about 0.95 c_s.

In order to investigate the effect of the tunnel buried depth on the tunnel radial stress, the radial stress of the tunnel at three buried-depths is presented in Fig. 6. It is clearly shown that the maximum dynamic stress decreases rapidly as the tunnel-buried depth increases. Comparisons between Fig. 6(a) and Fig. 6(b) show that the dynamic stress vanishes more rapidly versus the tunnel depth at a high load velocity.

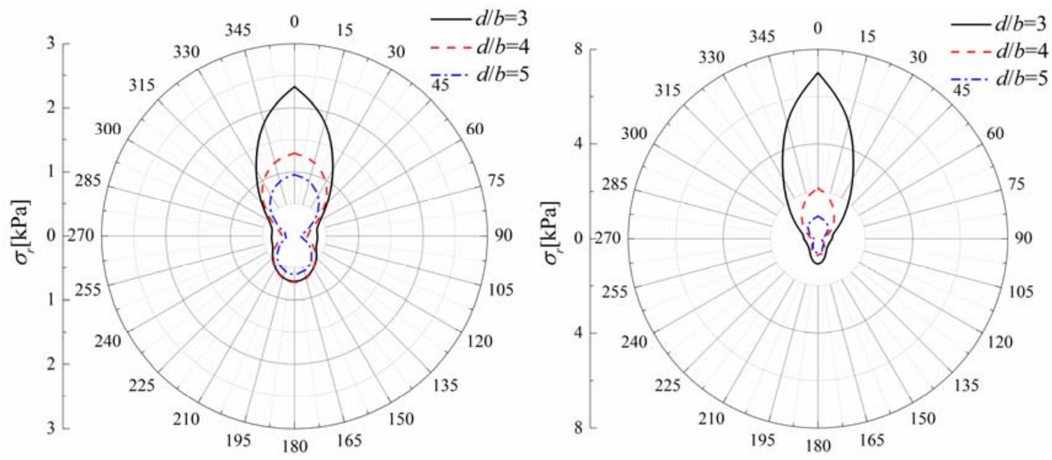

Fig. 6. The radial stress under different tunnel buried depth: (a) c=20 m/s and (b) c=100 m/s

To illustrate the effects of the tunnel-buried depth more clearly, Fig. 7 presents the maximum dynamic stress and velocity against the tunnel-buried depth. It is shown that the dynamic stress and vibration velocity decrease rapidly with the depth for both low and high load speeds. The effect of load speed on the dynamic response is weakened as the tunnel-buried depth increases. Fig. 7(a) gives the radial stress at the observation point A. When d/b=2, the radial stress of the observation point to a moving load of c=20m/s is 16kPa, which accounts for about 16% of the overburden stress here; as the load speed increases to 100m/s, the radial stress is 32kPa which accounts for about 32% of the overburden stress. Thus, for a shallowly-buried tunnel, the dynamic stress caused by a surface load cannot be ignored, especially when the traffic speed is high. Fig. 7(b) gives the maximum tunnel vibration velocity against the buried depth. It is also shown that the velocity decreases rapidly as the tunnel buried depth increases. Currently, there is no specification for vibration restriction of underground construction caused by surface traffic load. Thus, the present study adopts the vibration limit of 1.0×10^{-2} m/s according to the ISO specification (04866-2010) [7] which gives the allowable vibration of surface building caused by moving traffics. It is shown in Fig. 7(b) that the tunnel vibration exceeds the vibration limit 1.0×10^{-2} m/s when the tunnel is shallowly-buried tunnel for the certain traffic loading. When the tunnel-buried depth exceeds the critical depth d_c, the vibration of the tunnel will be attenuated to a value below the limit. The critical depth d_c is about 11.5 m for of the load speed 20 m/s and 16 m for the load speed of 100 m/s.

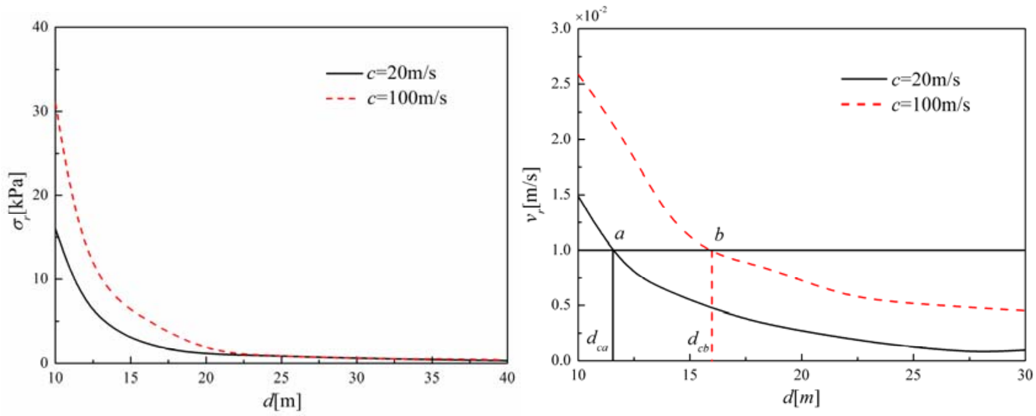

Fig. 7. The maximum responses at the tunnel vault against the tunnel buried depth (a) the vertical stress, (b) the vertical velocity

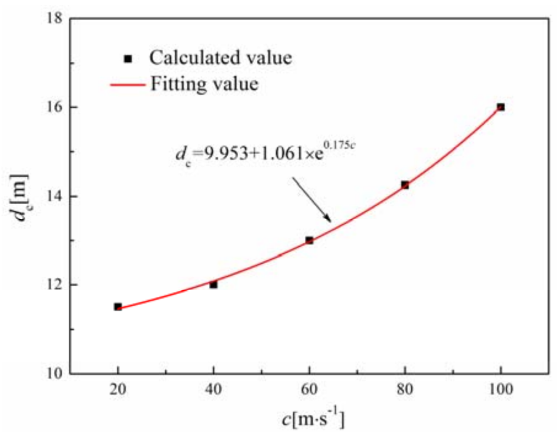

Fig. 8. The critical tunnel-buried depth against the velocity of the surface load

Fig. 8 shows the variation of the critical tunnel-buried depth with the change of load speed. It can be seen that the critical depth d_c grows exponentially as the load speed increases. This indicates that the dynamic magnification and the influence zone of the moving surface loads increases as the load speed increases.

4. Conclusion

In the present work, the impact of moving surface loads on the underground tunnel was investigated by a three-dimensional analytical model of a circular tunnel buried in the elastic half-space. A parametric analysis was performed for different moving speed and tunnel depth. The main conclusions of this paper are summarized as follows:

(1) The dynamic response of the tunnel generated by the moving surface load increases with the loading velocity, which reaches a peak value at the critical velocity of about 0.95 Vs. The effects of the load speed become minimized as the tunnel buried depth increases.

(2) The dynamic response of the tunnel can be greatly reduced as the tunnel buried depth increases. The critical tunnel-buried depth, exceeding which the tunnel vibration meets the allowable limit (given by ISO 04866), increases exponentially with the increase of the speed of moving surface load.

Acknowledgement

The authors are grateful to the support of National Key R&D Program of China （2016YFC0800200）, National Natural Science Foundation of China (Grant Nos. 51778571, 51578500, 51578426), and the European Union's Horizon 2020 MARIE SKLODOWSKA-CURIE RESEARCH AND INNOVATION STAFF EXCHANGE Program under the grant No 778360.

References

[1] Ba Z, Liang J, Lee V. 3D dynamic response of a multi-layered transversely isotropic half-space subjected to a moving point load along a horizontal straight line with constant speed, Int J Solid Struct 2016; 100: 427-445.

[2] Yang YB, Hsu LC. A review of researches on ground-borne vibrations due to moving trains via underground tunnels. Adv Struct Eng 2006; 9(3): 377-392.

[3] Forrest JA, Hunt HEM. A three-dimensional tunnel model for calculation of train-induced ground vibration. J Sound Vib 2006; 294(4-5): 678-705.

[4] Cai Y, Cao Z. Key technique for the construction of tunnel group under complicated geological conditions. Technique report; 2014, pp. 31-42.

[5] Yuan Z, Boström A, Cai Y. Benchmark solution for vibrations from a moving point source in a tunnel embedded in a half-space. J Sound Vib 2017; 387: 177-193.

[6] Hung HH, Yang YB. Analysis of ground vibrations due to underground trains by 25 D finite/infinite element approach. Earthquake Eng Eng Vib 2010; 9(3):327-335.

[7] ISO 04866: Mechanical vibration and shock —Vibration of fixed structures — Guidelines for the measurement of vibrations and evaluation of their effects on structures; 2010.

[8] Yuan Z, Boström A, Cai Y, Cao Z. Analytical wave function method for modelling a twin tunnel in a saturated poroelastic full-space. Comput Geotech 2019; 114: 103114-1-13.